Long-range charge order on the $Fe_3O_4(001)$ surface

I. V. Shvets, G. Mariotto,* K. Jordan, N. Berdunov, R. Kantor, and S. Murphy
SFI Trinity Nanoscience Laboratories, Physics Department, Trinity College, Dublin 2, Ireland
(Received 7 May 2004; revised manuscript received 4 August 2004; published 15 October 2004)

The Verwey transition in magnetite is of fundamental importance for the understanding of metal-insulator transitions but, in spite of being the subject of many studies over the last century, its nature is not fully understood. This is even more true in the case of the magnetite surface, where the low dimensionality plays an additional role in the determination of the Verwey transition temperature. We have atomically resolved the $(\sqrt{2}\times\sqrt{2})R45°$ reconstructed surface by scanning tunneling microscopy and we have modeled our experimental results by density functional theory calculations. We attribute the observed pattern to the charge ordering of Fe^{2+}-Fe^{2+} and Fe^{3+}-Fe^{3+} dimers. We propose a mechanism for the formation of this charge ordered surface and provide an explanation for the increase of the Verwey transition temperature at the (001) surface of magnetite.

DOI: 10.1103/PhysRevB.70.155406 PACS number(s): 71.30.+h, 71.38.Mx

I. INTRODUCTION

The Verwey transition is a metal-insulator transition that occurs in some ionic crystals as a change in electric conductivity and lattice symmetry. The Verwey transition temperature T_V in stoichiometric magnetite (Fe_3O_4) is around $T_V \simeq 125$ K. Below T_V, the electric conductivity drops by about two orders of magnitude and the lattice symmetry is lowered from cubic to monoclinic. Despite intensive research spanning almost a century, the nature of the Verwey transition is not completely understood. Various theoretical models, recently revised by Waltz,[1] have been proposed to explain the electron transport mechanism in the low- and high-temperature phases, and the sudden change in conductivity at the transition point. Among these are the models proposed by Wigner, Mott, the Hubbard-Mott transition, and the Anderson localization. Some models explain the Verwey transition as a complete order-disorder transition, either due to an ordering of the charges of the conducting electrons or of the electronic orbitals. Anderson estimated that a transition between a Verwey order and complete disorder would be expected for temperatures of the order of 10^4 K.[2] In order to explain the much lower transition temperature measured experimentally, Anderson proposed two different types of order: a long-range order (LRO) present at $T<T_V$ and a short-range order (SRO) that persists at $T>T_V$. He also postulated a condition for SRO, according to which the minimum lattice energy is achieved provided every tetrahedron formed by the nearest-neighbor octahedral sites is occupied by two Fe^{2+} and two Fe^{3+} ions.[2] An attempt to explain the Verwey transition as a consequence of the formation of bipolarons has also been proposed.[3] Bipolarons result from the attraction of polarons and are predicted to arise in the case of strong electron-phonon coupling for low-dimensional systems. A superstructure on the $Fe_3O_4(111)$ surface has been recently explained by Shvets *et al.* in terms of a giant localized polaron.[4]

Relatively little work has been done so far on the Verwey transition at the surface of magnetite single crystals or thin films, partly due to the fact that the experimental techniques employed to detect the Verwey transition, e.g., as nuclear magnetic resonance (NMR) and resistivity versus temperature measurements, are not surface sensitive. During the last two decades, the invention of scanning tunneling microscopy (STM) has boosted the area of surface physics and the study of low-dimensional systems. A STM study of the $Fe_3O_4(001)$ surface using ferromagnetic Fe tips, suggested that a charge frozen state persists at the surface at room temperature.[5,6] Since no long-range order was detected, the observed short-range order was classified as a Wigner glass. This result has been recently confirmed by another group.[7]

We have recently shown that long-range charge order sets in on the $Fe_3O_4(001)$ surface.[8] In this paper we interpret our experimental results in the light of density functional theory (DFT) calculations and we propose a mechanism for the formation of long-range charge order at a temperature well above T_V.

II. EXPERIMENT

Magnetite has the inverse spinel crystal structure. The conventional unit cell of magnetite contains 32 oxygen ions packed in the fcc lattice, 8 Fe ions placed at sites with tetrahedral oxygen coordination (*A* sites) and 16 Fe ions placed at sites with octahedral oxygen coordination (*B* sites). In stoichiometric magnetite the *A* site Fe ions are Fe^{3+} and the *B* site ones are equally likely to be Fe^{2+} and Fe^{3+}. The synthetic crystals used in this study were grown employing the skull melting technique[9] and characterized by powder x-ray diffraction (XRD) and resistance versus temperature measurements. A lattice constant of 8.40 ± 0.01 Å and a Verwey transition temperature of 108 K were determined. Raman spectra of these crystals were consistent with magnetite reference spectra and indicated that the crystals did not contain other phases of iron oxides. Magnetization measurements using a vibrating sample magnetometre resulted in the value of $M_S=100.9$ emu/g, in agreement with the value of magnetization of magnetite. The crystals were mechanically polished using diamond paste with grain size down to 0.25 μm and inserted into a ultra high vacuum (UHV) system after rinsing them with organic solvent. The final sample preparation, sur-

face characterization, and STM measurements were performed in the UHV system with a base pressure of $\sim 1 \times 10^{-10}$ mbar. The *in situ* preparation procedure consisted of a combination of Ar^+ ion sputtering, annealing in UHV and annealing in an oxygen partial pressure. The argon and oxygen exposure varied between 3600 and 7200 L, while the annealing temperature ranged between 850 ± 50 K and 990 ± 50 K. The final anneal stage varied between 2 and 10 h. This preparation procedure produces a contaminant-free surface, showing a sharp $(\sqrt{2} \times \sqrt{2})R45°$ low-energy electron diffraction (LEED) pattern. STM measurements were performed at room temperature using tips made of antiferromagnetic MnNi alloy.[10,11] STM measurement were carried out in constant-current mode and the sample was biased. A bias voltage ranging from +0.6 to +1 V and a tunneling current between 0.1 and 0.3 nA were the typical parameters used.

III. RESULTS AND DISCUSSION

A detailed study of the $Fe_3O_4(001)$ surface by means of STM, LEED, and Auger electron spectroscopy (AES) has been recently published by us in Ref. 8. For a better understanding of the present manuscript we will summarize here the main findings. The surface of the crystal is terminated at the octahedral plane, exhibiting a $(\sqrt{2} \times \sqrt{2})R45°$ superlattice, as shown by LEED. We have identified its origin in the charge ordering of the Fe cations at the *B* sites rather than in an ordered array of vacancies. Atomically resolved STM images show a dimerization of the Fe cations along the [110] direction. Two different types of dimers, which alternate along the [110] direction, are identified with Fe^{3+}-Fe^{3+} and Fe^{2+}-Fe^{2+} dimers, giving rise to a surface that is in a charge ordered state at room temperature. One cannot exclude a more complex scenario, where electrons are distributed at the *B* sites in other proportions. However, our results clearly exclude the possibility that all the Fe ions at *B* sites on the surface have identical electronic states consistent with a completely disordered condition. STM provide evidence of a highly regular structure with a 12 Å periodicity. In most cases the periodicity remained uninterrupted all throughout the terrace length, suggesting that LRO has set on the surface.

As discussed in Sec. II, the preparation conditions varied somewhat in terms of annealing temperature and gas exposures. Although AES and LEED provide evidence of a clean, $(\sqrt{2} \times \sqrt{2})R45°$ reconstructed surface for all the various combinations of preparation conditions, new STM data show a somewhat different arrangement of the dimers on the surface. This is shown in Fig. 1(a) where, instead of a constant 6 Å separation between atomic rows along the $[1\bar{1}0]$ direction, the Fe^{2+}-Fe^{2+} dimers are shifted by ~ 1 Å with respect to the Fe^{3+}-Fe^{3+} dimers. This is shown by the line-profile shown in Fig. 1(b).

In the following sections we shall discuss the possible mechanisms that can lead to the formation of Fe^{3+}-Fe^{3+} and Fe^{2+}-Fe^{2+} dimers. We will also discuss the reasons for the formation of long range order as opposed to a short range order quasiperiodicity.

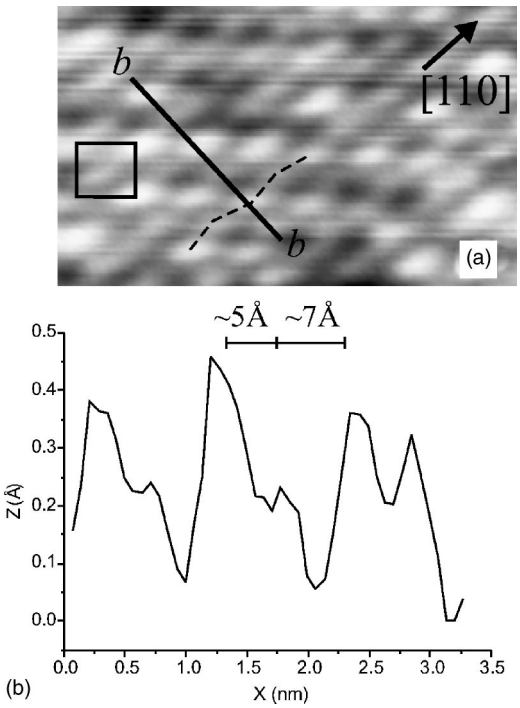

FIG. 1. (a) (130×150) Å^2 STM image. Spots of two different brightness are imaged, corresponding to dimers of Fe^{2+} and Fe^{3+} ions. The $(\sqrt{2} \times \sqrt{2})R45°$ superlattice is marked in (a). The line profile in (b)—taken along the line *b*-*b* of (a)—shows the alternating periodicity of 5 and 7 Å along the $[1\bar{1}0]$ direction.

A. Electronic configuration

The electron bands of Fe_3O_4 have been calculated using local-spin density calculations (LSDA) by Zhang and Satpathy[12] and using augmented plane wave (APW) calculations by Yanase and Siratori.[13] The three-band Hamiltonian formed by the t_{2g} $(xy, yz, zx,)$ orbitals on the *B* sublattice can be written as follows:

$$H = \sum_{i,j} \sum_{\mu,\nu=1}^{3} t_{ij}^{\mu\nu} c_{i\mu}^{+} c_{j\nu} + \sum_{i,j} \sum_{\mu,\nu=1}^{3} U_{i\mu,j\nu} \times n_{i\mu} n_{i\nu} + \sum_{i,j} V \times n_i n_j. \quad (1)$$

The second and third terms in Eq. (1) describe the on-site and intersite Coulomb energy terms, respectively. $n_{i\mu}$ is the number operator of the electron at the *i*th site of the orbital μ, where the orbital indices μ and ν take *xy*, *yz*, and *zx* values. n_i is the number operator for each site, i.e., $n_i = n_{ixy} + n_{iyz} + n_{izx}$. U and V are the on-site and intersite Coulomb interaction constants. Electron hopping between the orbitals μ and ν of octahedral Fe ions at the *i*th and *j*th sites is driven by the term $t_{ij}^{\mu\nu} c_{i\mu}^{+} c_{j\nu}$. Here $c_{i\mu}^{+}$ and $c_{j\nu}$ are the electron creation and annihilation operators of the electron of orbital μ at site *i* and of orbital ν at site *j*, respectively. The transfer integral is $t_{ij}^{\mu\nu}$. The results of both calculations of Refs. 12

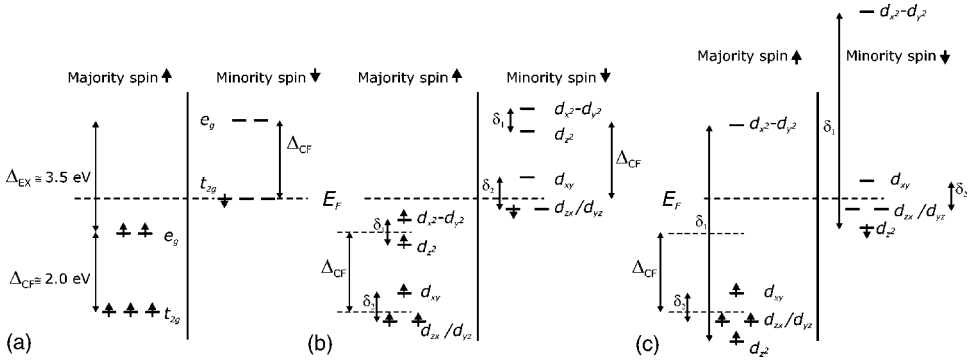

FIG. 2. (a) Schematic showing the splitting (Δ_{CF}) of a five-fold orbitally degenerate *d*-level of an Fe^{2+} ion in an octahedral crystal field. The splitting of the electronic band (Δ_{EX}) into a majority subband (spin-↑) and a minority subband (spin-↓) is also shown. (b) A further splitting (δ_1 and δ_2) occurs at the surface, where the symmetry is lowered because of a missing apical oxygen. The e_g doublet splits into the levels $d_{x^2-y^2}$ and d_{z^2}. The t_{2g} triplet splits, with the $d_{yz}-d_{zx}$ degenerate doublet lying lower than the d_{xy} level. (b) shows the case of a small split δ_1, $\delta_2 < \Delta_{CF}$ leaving the degenerate $d_{yz}-d_{zx}$ doublet as the lowest energy level for ↓ electrons. (c) shows the case of a large split for a Fe^{3+} ion. If $\delta_1 > \Delta_{CF}$, the d_{z^2} level may become lower in energy than the $d_{yz}-d_{zx}$ doublet. However, the $d_{yz}-d_{zx}$ doublet is still occupied by a single electron as the $d_{x^2-y^2}$ level in the spin ↑ subband moves up as a result of the same splitting and thus becomes vacant.

and 13 are in good agreement, showing an exchange splitting Δ_{EX} between the majority and minority subbands on the Fe atom of about 3.5 eV. The five-fold *d* levels are split into t_{2g} and e_g orbitals by the crystal field. The crystal-field splitting Δ_{CF} is approximately 2 eV for the Fe(*B*) atom, and few tenths of an electronvolts for the Fe(*A*) atom. The calculations show that the spin-↑ bands (majority spins) are semiconducting while the spin-↓ bands (minority spins) are metallic. It follows that only spin-↓ belonging to t_{2g} orbitals of Fe(*B*) are present at the Fermi level, while the O(*p*) orbitals lay well below the Fermi energy. A schematic of the Fe(*B*) electronic levels in the bulk is shown in Fig. 2(a). On the surface the band structure is altered. As we explained at the beginning of this section, our crystals are terminated at the *B* plane. Therefore, the coordination of the Fe(*B*) ions is lowered, since the apical oxygens are missing. This lowers the site symmetry from cubic to tetragonal, which leads to a splitting of the t_{2g} levels as shown in Fig. 2(b). The d_{yz} and d_{zx} orbitals lay lower than the d_{xy} orbital. The values of the nearest-neighbors transfer integrals $t_{ij}^{\mu\nu}$ were estimated in Ref. 14, with $t^{xy\text{-}xy} = -0.278$ eV, $t^{yz\text{-}yz} = 0.085$ eV, and $t^{zx\text{-}zx} = -0.035$ eV, while all the other configurations are $t_{ij}^{\mu\nu} = 0$.

B. Lattice deformation and charge ordering

An exact analytical solution of Eq. (1) can be obtained for any value of *t* and *U* provided that the system has one-dimensional (1D) geometry and that one electron is shared between two sites, e.g., there is an equal number of Fe^{2+} and Fe^{3+} ions. The analytical solution suggests that Fe^{2+} and Fe^{3+} ions should alternate along the 1D chains of *B* sites forming a-Fe^{2+}-Fe^{3+}-Fe^{2+}-Fe^{3+}-structure.[15] The *B* sites within the (001) surface of magnetite do in fact represent 1D chains. The *B* sites are arranged in lines aligned along the [110] and $[1\bar{1}0]$ directions. The separation between neighboring Fe ions along the lines (3 Å) is half of that in between the lines. Besides, there are two oxygen ions positioned in between the nearest Fe ions of any neighboring line. One can therefore conclude that electron hopping between the neighboring parallel lines is suppressed. Similarly, electron hopping between the surface and the bulk is suppressed as electron levels on the surface are shifted with respect to the bulk levels, due to the additional crystal field caused by a missing apical oxygen [see Figs. 2(a) and 2(b)]. Therefore, as electronic transport on the (001) surface takes place along one dimension, one can expect that Fe^{2+} and Fe^{3+} ions should form the Fe^{2+}-Fe^{3+}-Fe^{2+}-Fe^{3+} sequence along the [110] and $[1\bar{1}0]$ lines of *B* sites on the surface. We shall call this state the 1-1 pattern to differentiate it from the experimentally observed pattern of alternating pairs. The latter shall be called the 2-2 pattern. It is clear that the 1-1 pattern should indeed be the ground state, if only the Coulomb and Hubbard exchange interactions are taken into account, as all terms in Eq. (1) result in an energy increase for any deviation from the 1-1 pattern. However, our experimental results contradict this prediction. In the remainder of this chapter we shall discuss the mechanism that leads to the stabilization of the 2-2 pattern. We suggest that such a pattern is stabilized by lattice deformation and that the energy difference between the 1-1 and 2-2 patterns is compensated by a difference in the elastic energy. In other words the dimerization of Fe cations results in an energy gain (through electron-lattice interaction) that overweighs the energy penalty due to Coulomb repulsion and suppressed Hubbard exchange.

1. Jahn-Teller effect

One possible mechanism of electron-lattice interaction is the Jahn-Teller (JT) effect. It is only effective for the case of orbital degeneracy. In both cases of small and large splitting shown in Figs. 2(b) and 2(c), respectively, the high-spin Fe^{2+} (d^6) ions have such a degeneracy and therefore are subject to JT effect. At the same time, in both cases of small and large splitting, the Fe^{3+} ions are not degenerate. For a start it should be pointed that in both cases of small and large splitting, the Fe^{2+} ions have t_{2g} degenerate orbitals and these are known not to display a strong JT effect. Figure 3(a) shows

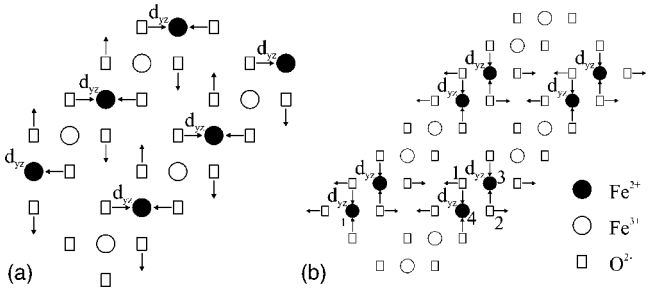

FIG. 3. (a) Schematic showing the expected Jahn-Teller deformations on the (001) surface of magnetite for the 1-1 pattern. The schematic illustrates the case for the $t^{yz\text{-}yz}$ transfer integral. (b) Schematic showing the expected Jahn-Teller deformations on the (001) surface of magnetite for the 2-2 pattern. The schematic illustrates the case for the $t^{yz\text{-}yz}$ transfer integral. The O anions labeled "1" and "2" are shared between the Fe^{2+} cations labeled "3" and "4.". The directions of anionic displacements due to cations 3 and 4 are shown by two arrows initiating at each of the anions 1 and 2.

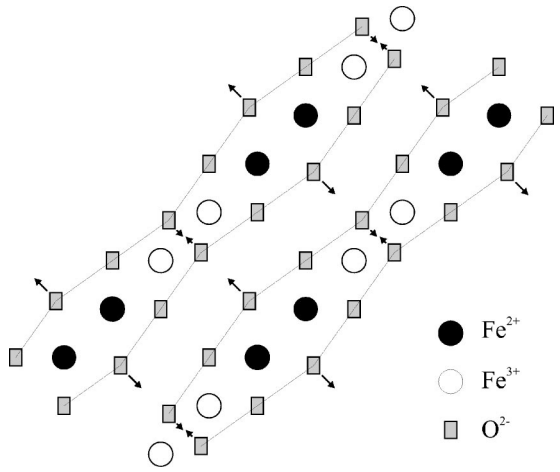

FIG. 4. Electron-lattice instability on the (001) surface of magnetite terminated at the *B* plane that favors the formation of the 2-2 pattern. The lattice deformation induces a splitting of the electron levels sufficient to induce a gain in energy that overcomes the Coulomb repulsion due to the pairing of Fe ions.

the JT distortion for the 1-1 pattern in the case of $t_{yz\text{-}yz}$-$t_{yz\text{-}yz}$ transfer integral. The case of the $t_{zx\text{-}zx}$-$t_{zx\text{-}zx}$ transfer integral is similar and can be obtained by rotation of deformation pattern shown in Fig. 3(a) by 90° degrees. One can appreciate that in the 1-1 pattern, the Fe^{2+} cations on the surface do not share nearest-neighbor oxygen anions. Therefore, displacement of each anion is determined by a single Fe cation.

The 2-2 pattern could be energetically more favorable than the 1-1 pattern provided the direction of displacement of a shared anion by the first cation is collinear with the one driven by the second cation. However, this is not the case for any of the possible configurations corresponding to the $t_{yz\text{-}yz}$, $t_{xy\text{-}xy}$ and $t_{zx\text{-}yz}$ transfer integrals. The case of a 2-2 pattern with the *yz*-*yz* orbital configuration is shown in Fig. 3(b). Anions marked with numerals 1 and 2 are shared between cations marked with numerals 3 and 4. The arrows initiating at each of the anions 1 and 2 indicate the directions of two anionic displacements caused by the cations 3 and 4. These are clearly not collinear. One can arrive to similar conclusions for 2-2 patterns with any of the other two configurations: $t_{xy\text{-}xy}$ and $t_{zx\text{-}yz}$ transfer integrals. Therefore, there is no basis for the onset of the collective JT distortions to explain the STM results obtained given the symmetry of the *B*-plane terminated (100) surface of magnetite.

2. Bipolaronic instability

To explain the results obtained, we favor another mechanism that, unlike JT distortions does not remove electron level degeneracy but still reduces the overall energy of the system through electron-lattice interaction. In this model a wave of anionic displacement induces a splitting of the electron levels sufficient to induce a gain in energy that overcomes the Coulomb repulsion due to the pairing of Fe ions. Given the localization of the electron charge and its strong interaction with the lattice, it may be appropriate to call the pair of Fe ions a localized bipolaron. Let us consider the case when the fifth 3*d* electron of the Fe^{3+} ion is located at the d_{z^2} orbital, corresponding to the crystal field splitting shown in Fig. 2(c). Moving anions closer to the Fe^{3+} ion or away from it changes the splitting between the $d_{x^2\text{-}y^2}$ and d_{z^2} levels. Therefore, the anionic displacement shown in Fig. 4 will lower the energy of the d_{z^2} level. Similar considerations apply to a pair of Fe^{2+} ions in the case of a small crystal field splitting [Fig. 2(b)], where the d_{zx}/d_{yz} levels are lowered in energy. This pattern is consistent with our STM images (see Fig. 1 and Ref. 8).

To support our interpretation of the STM data, we have performed DFT calculations using the CASTEP algorithm.[16] The local spin-density approximation (LSDA) based on ultrasoft pseudopotentials was used to optimize the surface geometry and to calculate the local density of states. A plane cutoff of 260 eV and a $(2\times2\times1)$ grid of *k* points were chosen. The calculations were performed for a slab of two unit cells and the electron density distribution was calculated for an energy range between the Fermi level and +1 V, to compare with our experimental settings. The results are shown in Fig. 5. The calculations show that Fe octahedral ions form pairs along the [110] direction, and that the dimerization is stabilized by lattice strain. Our calculations do not show a significant difference in the electron density distribution between pairs of Fe ions, mainly due to two reasons. First, a two unit cell slab is likely to be too small to resolve the 12 Å periodicity. However, we are not able to model a larger slab, due to computational limitations. Second, in our calculations we were not able to force a complete localization of the sixth d^6 electrons at the *B* sites.

In line with this model, the Verwey transition at the surface can be considered as a bipolaron blocking temperature T_b. There is a distinct possibility that above T_b the charge transport on the surface takes place by means of mobile bipolarons, i.e., mobile bosons. As our STM measurements were taken at room temperature, one can further conclude that T_b is above room temperature. In other words, the Verwey temperature on the (001) surface is much greater than the one in the bulk. The increase of T_V on the surface can be explained as follows. We can consider electrons in any of the

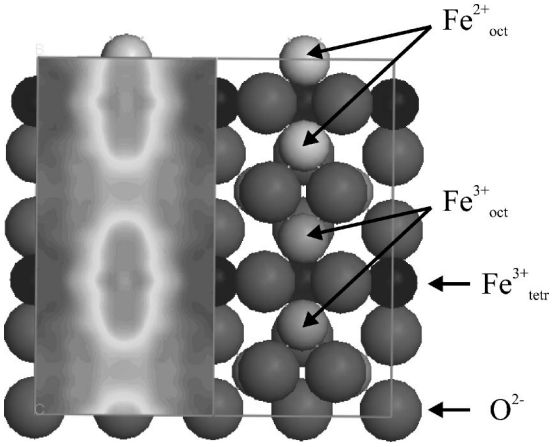

FIG. 5. DFT calculations for a two unit cell slab of a *B*-terminated magnetite crystal. A configuration in which pairs of Fe^{2+} and Fe^{3+} ions at *B* sites alternate along the [110] directions can be stabilized by a deformation of the lattice. The energy density distribution shows a clear dimerization, in good agreement with our STM results.

[110] and $[\bar{1}10]$ chains of *B* sites Fe ions as a separate system. Indeed, the electron transport on the (001) surface occurs along the [110] and $[\bar{1}10]$ directions, while transport between the surface and the bulk occurs along the remaining four directions: [011], $[01\bar{1}]$, [101], and $[10\bar{1}]$. However, we suggest that the transport between the surface and the bulk is hindered because cationic electron levels in the bulk and at the surface correspond to different energies (see Fig. 2). This implies that hopping between the surface and the bulk is suppressed as hopping is only effective between degenerate levels. Our analysis of T_b is semiquantitative and is based on the comparison of free energies

$$F = E - TS. \tag{2}$$

in the bipolaron-ordered (BO) and non-ordered (NO) states, called here F_{BO} and F_{NO}, where S is the entropy associated with a multiplicity of states due to mobile bipolarons. In our analysis we assume that in the NO state the bipolarons are already formed but they are mobile. Of these two states, the state chosen by the system at any given temperature is the one that corresponds to the lower free energy. As in the BO state the entropy associated with bipolaron states can be assumed to be zero (just one pattern corresponding to the ground state contributes to the multiplicity function), then $F_{BO}=E_{BO}$. In the same way $F_{NO}=E_{NO}-TS$. Therefore, as at the BO-NO transition $F_{BO}=F_{NO}$, the transition temperature can be estimated as $T=(E_{NO}-E_{BO})/S$. We shall show that the transition between the BO and NO states on the surface should occur at a higher temperature than in the bulk, i.e., $(T_b)_{surface} > (T_b)_{bulk}$.

First, we will give a qualitative explanation of why the energy difference $\Delta E_{total}=E_{NO}-E_{BO}$ between NO and BO states should be greater at the surface than in the bulk, causing an increase of T_V at the surface. From the Hamiltonian of Eq. (1) we can see that the energy of each electron has two contributions: a negative one from the transfer integral $\Delta E_{transfer}$ (first term), and a positive one from the Coulomb interaction energy $\Delta E_{Coulomb}$ (second and third terms). The total energy of the electron can therefore be written as

$$\begin{aligned}\Delta E_{total} &= \Delta E_{transfer} + \Delta E_{Coulomb} \\ &= (E_{NO} - E_{BO})_{transfer} + (E_{NO} - E_{BO})_{Coulomb}.\end{aligned} \tag{3}$$

The transfer integral essentially underlines the uncertainty principle: As the current carriers become more localized, their energy increases. For each carrier placed at a *B* site in the bulk, transport is possible in three dimensions, along the $\langle 110 \rangle$ set of directions. On the other hand, electrons placed at a *B* site at the surface can only move along one dimension. Therefore, charge freezing in the bulk results in an energy increase of the order of $3\hbar^2/2m\Delta x^2$, where Δx is the size of the area of the electron localization, while at the surface the energy increase is only $\hbar^2/2m\Delta x^2$. In other words, electron hopping at the surface is restricted to one dimension even in the NO state. Therefore, as the negative contribution $\Delta E_{transfer}$ is smaller at the surface, the energy difference $\Delta E_{transfer}$ on the surface should be greater than in the bulk. The Coulomb interaction energy $\Delta E_{Coulomb}$ at the surface is greater than in the bulk, due to the missing apical oxygen atoms, which lower the symmetry from cubic to tetrahedral. In conclusion, $(\Delta E_{total})_{surface} > (\Delta E_{total})_{bulk}$.

Second, we will show that the value of the entropy S normalized per one electron is smaller at the surface than in the bulk, leading to a further increase of T_b. To compare the entropies of the surface and the bulk we estimate the number of ground states for systems of different dimensionality. The entropy can be calculated as

$$S = k \ln W. \tag{4}$$

where W is the number of states equally accessible to the system. We follow the approach applied by Anderson to estimate the electron entropy in bulk Fe_3O_4.[2] The Anderson model is based on the argument that the energy of the entire electron system in magnetite is essentially determined by short-range order. As long as each tetrahedron of *B* sites contains two Fe^{2+} and two Fe^{3+} ions (Anderson condition), the state is attributed to the group of ground states regardless of the long-range order arrangement. Therefore, in this model the ground state should be heavily degenerate if a substantial number of permutations fulfill the Anderson condition. The number of states W in the bulk is estimated as $(3/2)^{N/2}$, where N is the number of *B* sites in the lattice.[2] Therefore, a value of $S_{bulk}=R/2\ln(3/2)=0.81R$ is calculated per mole of octahedral sites. This rather large entropy results from a particular arrangement of the *B* sites in the spinel crystal structure, which fulfils the Anderson condition for a large number of charge arrangements.

We can now apply the same approach to the (001) surface of $Fe_3O_4(001)$ exhibiting the experimentally observed 2-2 pattern. Two cases must now be considered. These are shown in Figs. 6(a) and 6(b). Both figures show the topmost Ander-

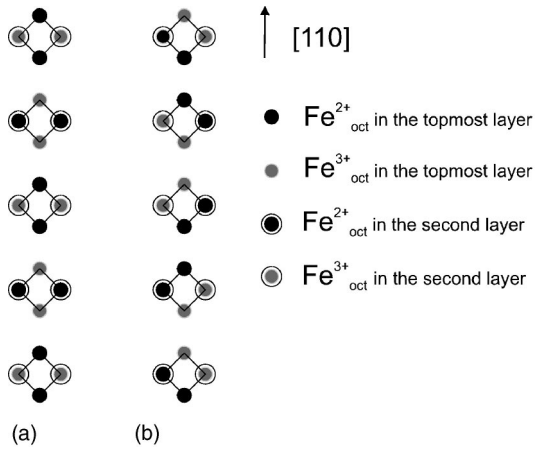

FIG. 6. Top view of octahedral chains of Fe cations. The first two layers are shown, and the tetrahedrons formed by nearest-neighbors octahedral sites are marked by black solid lines. The consideration is based on fulfilling Anderson's condition and the experimentally observed pattern of charge pairs on the surface. Two cases can be distinguished. (a) Pairs of Fe^{2+} ions in the topmost layer and Fe^{3+} ions in the second topmost layer belong to the same Anderson tetrahedron. (b) Each pair of Fe^{2+} ions on the surface is shared between two Anderson tetrahedrons. The topmost *B* sites are indicated as single circles, while the *B* sites in the second layer are indicated in double lines.

son tetrahedron formed by the topmost and second topmost layers of *B*-site Fe ions. In the first case [Fig. 6(a)] the pair of Fe^{2+} ions in the topmost layer and Fe^{3+} ions in the second topmost layer belong to the same Anderson tetrahedron. In this case there is only one state that fulfils this condition for each pair of Fe^{2+} and Fe^{3+} ions on the surface. In the second case, each pair of Fe^{2+} ions on the surface is shared between two Anderson tetrahedrons [Fig. 6(b)]. In this case there are two possible states for each of the N/2 pairs of Fe^{2+} ions on the surface fulfilling the Anderson condition. Thus the total number of states is $W=2N/2$, giving an entropy value of $S_{\text{surface}}=R/2\ln 2=0.34R$. Since $(\Delta E_{\text{total}})_{\text{surface}}>(\Delta E_{\text{total}})_{\text{bulk}}$ and $S_{\text{surface}}<S_{\text{bulk}}$, it follows that $(T_b)_{\text{surface}}>(T_b)_{\text{bulk}}$. A higher transition temperature at the surface of magnetite explains why long-range order can still set in at room temperature.

3. Other models

It should be pointed out that some of our results could also be explained by alternative models. It was recently proposed by Seo *et al.*[14] that the strong electronic correlation at the *B* sites can create an orbital ordering (OO) state with a 1D electronic structure. Such a system has a Peierls instability with two times the interatomic distance,[14,17] in agreement with our STM results. The 2-2 pattern may also be driven by a regular array of oxygen vacancies on the surface. The removal of oxygen ions results in the creation of inequivalent *B* sites on the magnetite surface. As a consequence, two neighboring Fe_{oct} sites are adjacent to the vacancy and two neighboring Fe_{oct} sites are still fully surface coordinated by O^{2-} ions. Therefore, alternating pairs of *B* sites with different energies are created along the [110] direction, which may drive the dimerization of the Fe ions. The O^{2-} vacancies have a virtual positive charge and so in order to minimize the surface energy the Fe^{2+} ions will occupy the two sites adjacent to these O^{2-} vacancies and the Fe^{3+} ions will occupy the pair of sites furthest from the vacancy. The virtual positive charge of an O^{2-} vacancy may also explain the relaxation observed on the surface. The shifting along the $[1\bar{1}0]$ direction, marked by the dashed zigzag line in Fig. 1(a), could result from the repulsive effect of the array of O^{2-} vacancies on the pairs of Fe^{2+} ions. Wavelike rows of Fe ions were observed by Stanka *et al.* However, neither the dimer formation nor the difference between Fe^{2+} and Fe^{3+} ions were observed in this previous study.[18] In our model, the oxygen vacancies create an energy barrier to electron hopping between the octahedral surface sites, resulting in long range order on the surface. The introduction of O^{2-} vacancies is also favorable in terms of reducing the surface polarity of magnetite (001).

IV. CONCLUSIONS

In this study we have analyzed the $(\sqrt{2}\times\sqrt{2})R45°$ reconstructed surface of $Fe_3O_4(001)$ synthetic crystals by STM and LEED. Our results provide evidence of the formation of Fe^{2+}-Fe^{2+} and Fe^{3+}-Fe^{3+} pairs along the [110] rows of *B* sites, in agreement with the results of other groups.[5,7] However, we observe a different shift between adjacent Fe rows and most importantly, the set in of long-range order. We propose a mechanism to explain the observed charge ordered surface based on electron-lattice interaction. Our model is supported by DFT calculations, which show that the dimerization of Fe ions at *B* sites can be stabilized by a deformation of the lattice. In our model, the dimerization of Fe cations and the deformation of the oxygen fcc lattice lead to a lowering of the electron levels and to a consequent gain in energy. This energy gain overcomes the energy penalty due to a higher Coulomb repulsion caused by the pairing of Fe cations and to the suppression of the Hubbard exchange caused by the localization of electron charges. Given the strong electron-lattice interaction and the localization of the sixth d^6 electrons on the Fe^{2+} ions, we propose that the charge ordering at the (001) surface of magnetite is caused by localized bipolarons. Furthermore, we propose that the Verwey transition at the (001) surface of magnetite is much higher than in the bulk. This is essentially due to the lower dimensionality of the surface, which hinders electron transport between the bulk and the surface itself.

*Electronic address: mariotl@tcd.ie

[1] F. Waltz, J. Phys.: Condens. Matter **14**, R285 (2002).
[2] P. W. Anderson, Phys. Rev. **102**, 1008 (1956).
[3] B. K. Chakraverty, Philos. Mag. B **42**, 473 (1980).
[4] I. V. Shvets, N. Berdunov, G. Mariotto, and S. Murphy, Europhys. Lett. **63**, 867 (2003).
[5] R. Wiesendanger, I. V. Shvets, D. Bürgler, G. Tarrach, H. J. Güntherodt, J. M. D. Coey, and S. Gräser, Science **255**, 583 (1992).
[6] J. M. D. Coey, I. V. Shvets, R. Wiesendanger, and H.-J. Güntherodt, J. Appl. Phys. **73**, 6742 (1993).
[7] R. Koltun, M. Herrmann, G. Güntherodt, and V. A. M. Brabers, Appl. Phys. A: Mater. Sci. Process. **73**, 49 (2001).
[8] G. Mariotto, S. Murphy, and I. V. Shvets, Phys. Rev. B **66**, 245426 (2002).
[9] J. E. Keem, H. R. Harrison, R. Aragon, and J. M. Honig, Inorg. Synth. **22**, 43 (1984).
[10] S. Murphy, J. Osing, and I. V. Shvets, Appl. Surf. Sci. **144–145**, 497 (1999).
[11] S. F. Ceballos, G. Mariotto, S. Murphy, and I. V. Shvets, Surf. Sci. **523**, 131 (2003).
[12] Z. Zhang and S. Satpathy, Phys. Rev. B **44**, 13 319 (1991).
[13] A. Yanase and K. Siratori, J. Phys. Soc. Jpn. **53**, 312 (1984).
[14] H. Seo, M. Ogata, and H. Fukuyama, Phys. Rev. B **65**, 085107 (2002).
[15] E. H. Lieb and F. Y. Wu, Phys. Rev. Lett. **20**, 1445 (1968).
[16] M. D. Segall, P. J. D. Lindan, M. J. Probert, C. J. Pickard, P. J. Hasnip, S. J. Clark, and M. C. Payne, J. Phys.: Condens. Matter **14**, 2717 (2002).
[17] J. Bernasconi, M. J. Rice, W. R. Schneider, and S. Strässler, Phys. Rev. B **12**, 1090 (1975).
[18] B. Stanka, W. Hebenstreit, U. Diebold, and S. A. Chambers, Surf. Sci. **448**, 49 (2000).